Dynamics, thermodynamics, and phase transitions of classical spins interacting through the magnetic field

Debarshee Bagchi,* Renato Pakter,† and Yan Levin‡
Instituto de Física, UFRGS, Caixa Postal 15051, CEP 91501-970 Porto Alegre, Rio Grande do Sul, Brazil

(Received 18 January 2018; revised manuscript received 16 March 2018; published 29 May 2018)

We introduce and study a one dimensional model of classical planar spins interacting self-consistently through magnetic field. The spins and the magnetic field evolve in time according to the Hamiltonian dynamics which mimics that of a free electron laser. We show that by rescaling the energy due to magnetic field inhomogeneity, in equilibrium, this system can be mapped onto a model very similar to the paradigmatic globally coupled Hamiltonian mean-field (HMF) model. The system exhibits a continuous equilibrium phase transition from paramagnetic to ferromagnetic phase, however unlike HMF, we do not see any magnetized quasistationary states.

DOI: 10.1103/PhysRevE.97.052140

I. INTRODUCTION

Long-range interactions are ubiquitous in nature and can be found at all length scales, from cosmology [1] to nanotechnology [2]. Systems with long-range interactions are a challenge to study since, in the thermodynamic limit, they deviate dramatically from short-range interacting systems. In the thermodynamic limit, the conventional formalism of the Boltzmann-Gibbs statistical mechanics does not apply to isolated systems with long-range interactions, which become trapped in nonequilibrium quasistationary states (QSSs). Many intriguing dynamic and thermodynamic properties of long-ranged interacting models have been found. These range from ergodicity breaking, equilibrium and nonequilibrium phase transitions, QSSs, non-Maxwellian velocity distribution, negative specific heat, etc.; see reviews [3–6].

An exactly solvable—in equilibrium—paradigmatic model of a system with long-range interactions which has been extensively studied over the last two decades is the Hamiltonian mean-field (HMF) model [7,8]. However, despite its simplicity and usefulness in understanding many properties of long-range interacting systems, the HMF model is pathological, in the sense that perturbations propagate instantaneously between any two points. In a more physically realistic model one expects that there is no instantaneous action at a distance, and perturbation should propagate in space and time. With this in mind, we introduce and study a model of inertial planar spins on a one dimensional lattice interacting through a spatially and temporally varying magnetic field. The field acting on a spin is generated by all the spins in the system. Thus although the spins do not directly interact with each other, they interact through the magnetic field which they produce. This indirect interaction mediated by the field precludes instantaneous action at a distance, making the dynamics physically realistic. We show that by tuning the energy cost of inhomogeneity of magnetic fields, this one dimensional classical model undergoes a paramagnetic to ferromagnetic phase transition.

The paper is organized as follows. In Sec. II we introduce the model and show that at equilibrium, in the thermodynamic limit, with a suitable scaling of the coupling parameters it can be mapped onto a model similar to the HMF. Next in Sec. III we discuss the numerical approach and present the results obtained from simulations showing evidence of dynamical slowing down in the large system size limit and existence of a paramagnetic to ferromagnetic phase transition. A summary of results is presented in Sec. IV.

II. MODEL AND THE ANALYTICAL RESULTS

We consider a one dimensional lattice with planar spins $\vec{S}_i \equiv \{S_x, S_y\}_i$, at each site i, where $1 \leqslant i \leqslant N$, with N being the system size. Each spin is coupled to the field denoted by $\vec{h}_i \equiv \{h_x, h_y\}_i$ which is the magnetic field produced by all the $\vec{S}_j$ spins. The Hamiltonian of this self-consistent interacting spin model (SCISM) under periodic boundary conditions is

$$\mathcal{H} = \sum_i \left\{ \frac{p_i^2}{2} - \vec{h}_i \cdot \vec{S}_i + \frac{1}{2}\gamma \vec{h}_i^2 + \frac{1}{2}\rho(\vec{h}_i - \vec{h}_{i+1})^2 \right\}, \quad (1)$$

where γ, ρ are constants. The spin variables are all assumed to have a fixed length $|\vec{S}_i| = 1$ and a unit "mass"; their orientation and conjugate momentum are denoted by an angle variable $0 \leqslant \theta_i \leqslant 2\pi$ and momentum p_i, respectively. The magnetic field components $\{h_x, h_y\}$ are also assumed to be conjugate variables and as such follow the Hamiltonian dynamics. The dynamics for the magnetic field is motivated by the analogous behavior found in the free electron laser (FEL), where the magnetic field corresponds to the complex amplitude of the electromagnetic wave [9–11]. The equations of motion for the sets of variables $\{p_i, \theta_i\}$ and $\{h_{xi}, h_{yi}\}$ are

$$\dot{\theta}_i = \frac{\partial \mathcal{H}}{\partial p_i}, \quad (2)$$

$$\dot{p}_i = -\frac{\partial \mathcal{H}}{\partial \theta_i}, \quad (3)$$

*debarshee@cbpf.br
†pakter@if.ufrgs.br
‡levin@if.ufrgs.br

$$\dot{h_{xi}} = \frac{\partial \mathcal{H}}{\partial h_{yi}}, \tag{4}$$

$$\dot{h_{y_i}} = -\frac{\partial \mathcal{H}}{\partial h_{xi}}, \tag{5}$$

which, written explicitly, yield

$$\dot{\theta}_i = p_i, \tag{6}$$

$$\dot{p}_i = -h_{xi}\sin\theta_i + h_{y_i}\cos\theta_i, \tag{7}$$

$$\dot{h_{xi}} = -\sin\theta_i + \gamma h_{y_i} + \rho\left(2h_{y_i} - h_{y_{i+1}} - h_{y_{i-1}}\right), \tag{8}$$

$$\dot{h_{y_i}} = \cos\theta_i - \gamma h_{xi} - \rho(2h_{xi} - h_{xi+1} - h_{xi-1}). \tag{9}$$

The Hamiltonian Eq. (1) can be expressed in terms of the lattice Laplacian operator

$$\mathcal{H} = \sum_i \left\{ \frac{p_i^2}{2} - \vec{h}_i \cdot \vec{S}_i + \frac{1}{2}\gamma \vec{h}_i^2 - \frac{1}{2}\rho \vec{h}_i \cdot \triangle \vec{h}_i \right\}, \tag{10}$$

where $\triangle \vec{h}_i = \vec{h}_{i+1} + \vec{h}_{i-1} - 2\vec{h}_i$. Similar to FEL, besides the energy, the dynamics also conserves the total momentum of the system,

$$J = \sum_i \left\{ p_i - \frac{|\vec{h}_i|^2}{2} \right\}. \tag{11}$$

After a sufficiently large time, this system will relax to an equilibrium state described by the Boltzmann-Gibbs statistics with partition function

$$Z = \int \prod_i dp_i d\vec{S}_i d^2 h_i e^{-\beta\mathcal{H} - \beta\alpha J}, \tag{12}$$

where α and β are the Lagrange multipliers. In the canonical ensemble β corresponds to the temperature of the reservoir, and α is determined by the condition of momentum conservation

$$\langle p \rangle - \frac{\langle |\vec{h}|^2 \rangle}{2} = \frac{J_0}{N}, \tag{13}$$

where J_0 is the initial momentum and $\langle \ldots \rangle$ indicates the average over the lattice sites. In most of the simulations presented in this paper we will start with zero initial magnetic field and with $\langle p \rangle = 0$ at $t = 0$, so that $J_0 = 0$. Writing the effective Hamiltonian as

$$\mathcal{H}_{\text{eff}} = \mathcal{H}_0 + \sum_i \left\{ \frac{p_i^2}{2} + \alpha p_i - \vec{h}_i \cdot \vec{S}_i \right\}, \tag{14}$$

where

$$\mathcal{H}_0 = \sum_i \left\{ \frac{1}{2}(\gamma - \alpha)\vec{h}_i^2 - \frac{1}{2}\rho \vec{h}_i \cdot \triangle \vec{h}_i \right\}, \tag{15}$$

the partition function, Eq. (12), can be expressed as

$$\begin{aligned} Z &= Z_0 \int \prod_i dp_i d\vec{S}_i e^{-\beta \sum_i \{p_i^2/2 + \alpha p_i\}} \langle e^{\beta \sum_i \vec{h}_i \cdot \vec{S}_i} \rangle_0 \\ &= Z_0 \int \prod_i dp_i d\vec{S}_i e^{-\beta \sum_i \{p_i^2/2 + \alpha p_i\} + (\beta^2/2)\sum_{i,j} \langle (\vec{h}_i \cdot \vec{S}_i)(\vec{h}_j \cdot \vec{S}_j) \rangle_0}, \end{aligned} \tag{16}$$

where $Z_0 = \int \prod_i d^2 h_i e^{-\beta \mathcal{H}_0}$ and $\langle \ldots \rangle_0$ corresponds to the thermal average with respect to the Hamiltonian $\mathcal{H}_0$. To calculate the average appearing in the exponential, we Fourier transform the magnetic field,

$$\vec{h}(k) = \sum_j^N \vec{h}_j e^{-ikj}. \tag{17}$$

The inverse transform is

$$\vec{h}_j = \int_{-\pi}^{\pi} \frac{dk}{2\pi} \vec{h}(k) e^{ikj}. \tag{18}$$

In the thermodynamic limit $N \to \infty$, the noninteracting part of the Hamiltonian can then be diagonalized in the Fourier space,

$$\mathcal{H}_0 = \frac{\gamma_R}{2} \int_{-\pi}^{\pi} \frac{dk}{2\pi} |\vec{h}(k)|^2 - \rho \int_{-\pi}^{\pi} \frac{dk}{2\pi} (\cos k - 1) |\vec{h}(k)|^2, \tag{19}$$

where $\gamma_R = \gamma - \alpha$, and the thermal average $\langle \ldots \rangle_0$ can be evaluated explicitly,

$$Z = Z_0 \int \prod_l dp_l d\vec{S}_l e^{-\beta \sum_l \{p_l^2/2 + \alpha p_l - (1/2)\sum_j V_{lj} \vec{S}_l \cdot \vec{S}_j\}}, \tag{20}$$

where

$$V_{lj} = \int_{-\pi}^{\pi} \frac{dk}{2\pi} \frac{e^{ik(l-j)}}{\gamma_R - 2\rho(\cos k - 1)} \tag{21}$$

$$\approx \frac{1}{2\sqrt{\gamma_R \rho}} \exp\{-\sqrt{\gamma_R/\rho}(l - j)\}. \tag{22}$$

In the last equation we have used $\cos k \approx 1 - k^2/2$ to perform the integration, which is valid for large ρ, since in this limit most of the contribution to the integral comes from small k. The potential in Eq. (22) has the range of interaction proportional to $\sqrt{\rho/\gamma_R}$. If we rescale the magnetic field inhomogeneity coupling constant as $\rho = \rho_0 N^2$ ($\rho_0 > 0$ is a constant), then from Eq. (22) we obtain

$$V_{lj} \approx \frac{1}{2N\sqrt{\gamma_R \rho_0}} \exp\{-\sqrt{\gamma_R/\rho_0}(l - j)/N\}. \tag{23}$$

In order to perform molecular dynamics simulations with this interacting spin model we define an effective Hamiltonian,

$$\mathcal{H}' = \sum_i \frac{p_i^2}{2} + \alpha p_i - \frac{1}{2}\sum_i \sum_j V_{ij} \vec{S}_i \cdot \vec{S}_j. \tag{24}$$

For $N \to \infty$, the above spin-spin interaction energy in Eq. (24) is similar to the paradigmatic HMF model where all the spins interact with each other with equal strength [12,13]. The linear term in momentum provides the drive which originates from the transfer of part of the angular momentum to the magnetic field in the original SCISM model. At thermodynamic equilibrium we find $\langle p \rangle = -\alpha$. Therefore, we expect to see the similar equilibrium behavior of the SCISM and of the reduced model if α is set to $-\langle p \rangle$ obtained in the equilibrium state of the SCISM model. Note that the two models are not precisely the same, since in the definition of $\mathcal{H}'$, we have neglected the additive constant $-\ln(Z_0)/\beta$ related to the free energy of the magnetic field. Nevertheless, we

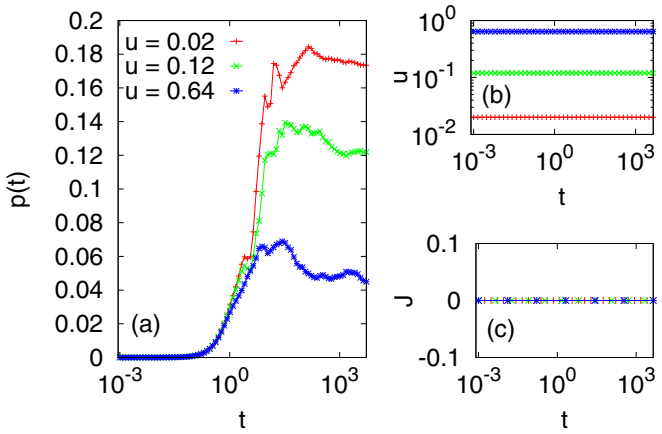

FIG. 1. (a) Evolution of the (cumulative) average momentum $p(t)$ with time t for different values of energy density u. The conservation of the energy density u and the angular momentum J is shown in (b) and (c) respectively for the same u values as in (a). Here $N = 100$ and $\rho = \rho_0 N^2$ with $\rho_0 = 0.02$.

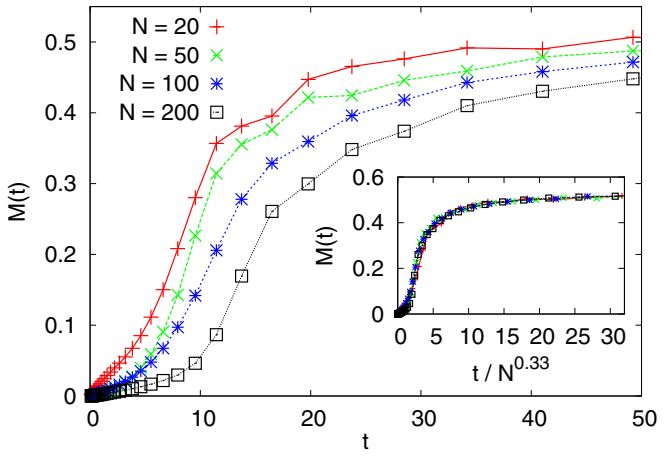

FIG. 2. Evolution of the magnetization $M(t)$ with time t for different values of N with the rescaling $\rho = \rho_0 N^2$. The inset shows the same data with the x axis rescaled as $t \to t/N^{0.33}$. The energy density is $u = 0.05$ and $\rho_0 = 1.0$.

speculate that the SCISM after rescaling of the inhomogeneity coupling parameter ($\rho = \rho_0 N^2$) should be very similar to a driven HMF model, and in particular should have an equilibrium paramagnetic to ferromagnetic phase transition. The interesting question that we would like to explore in this paper is if the model also has a nonequilibrium dynamical QSS.

III. RESULTS FROM SIMULATION

A. Dynamical properties

We first study the dynamical properties of the SCISM model described by the Hamiltonian Eq. (1) using numerical integration of the equations of motion, Eqs. (6)–(9). To integrate the equations numerically we employ a Runge-Kutta algorithm with adaptive time step that uses embedded fifth order and sixth order Runge-Kutta estimates to compute the solution and the relative error [14]. The initial conditions for the angle variable θ_i are chosen equidistantly in the range $0 < \theta_i < 2\pi$, so that the initial magnetization is $m = 0$ at $t = 0$. The spin momenta p_i are chosen randomly from a uniform distribution in the range $0 < p_i < p_m$, such that for every particle with momentum p there is another particle with momentum $-p$; we always have an even number of spins in our system so that the *initial* average spin momentum is strictly zero. Unless otherwise mentioned, the initial magnetic field components are chosen as $(h_x, h_y) = (0,0)$ at all the sites. Also, for all the simulation results presented in the following we have set the parameter γ to unity.

We begin by verifying that the conservation of the total energy per spin u and the total angular momentum J are obeyed by our numerical integration scheme and the average momentum $\langle p \rangle$ indeed saturates to a finite value at large times as we have argued in the previous section. In Fig. 1(a) we show the time evolution of the cumulative average momentum defined as

$$p(t) = \frac{1}{t}\int_0^t \langle p(t')\rangle dt', \tag{25}$$

where $\langle p \rangle = \sum_i p_i/N$, and observe that at large time we obtain a saturation (statistically). The energy density $u = \langle \mathcal{H} \rangle / N$ and the total momentum J (for our choice of initial conditions $J = 0$) both remain conserved throughout the simulation, ensuring that our numerical scheme satisfies the two conservation laws. The evolution of $\langle p \rangle$ also gives us an estimate of the equilibration time $t_{\rm eq}$ of the system and all equilibrium properties that we subsequently present are computed only after the system has evolved past $t_{\rm eq}$.

We are interested to see how SCISM evolves towards equilibrium when the coupling constant of the magnetic field inhomogeneity is scaled as $\rho = \rho_0 N^2$, and also if there are any dynamical and thermodynamical phase transitions. To explore this we compute the instantaneous magnetization m defined as

$$m = \left[m_x^2 + m_y^2\right]^{1/2}, \tag{26}$$

where $m_x = \frac{1}{N}\sum_i \cos\theta_i$ and $m_y = \frac{1}{N}\sum_i \sin\theta_i$.

In Fig. 2 we present the cumulative magnetization $M(t)$ [similar to Eq. (25)]

$$M(t) = \frac{1}{t}\int_0^t m(t')dt', \tag{27}$$

for different values of the system size N, while maintaining the $\rho = \rho_0 N^2$ scaling and energy per spin $u = \langle \mathcal{H} \rangle / N$. We see that starting from an initially paramagnetic state the system relaxes to a ferromagnetic state. As the system size increases, however, the magnetization M takes a longer time to saturate to the equilibrium value. In the inset of Fig. 2 we show that if the time t is rescaled as t/N^α all the data points for different N collapse onto a single curve. The exponent is found to be $\alpha \approx 0.33$. This indicates that a thermodynamically large system, $N \to \infty$, will take an infinite amount of time to relax to equilibrium, remaining trapped in the initial paramagnetic state. This is similar to what one encounters in the HMF model where the equilibration time t grows algebraically with the system size as [15] $t \sim N^2$ and thus a thermodynamically large HMF will never relax to the Boltzmann-Gibbs (BG) equilibrium state. Note that such dynamical slowing down does not arise if the parameter ρ is not scaled in the manner described above. This

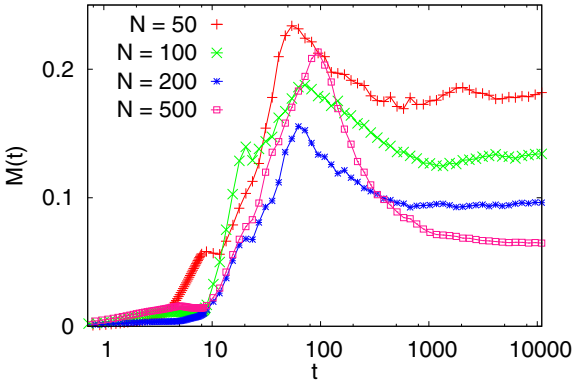

FIG. 3. Evolution of the magnetization $M(t)$ with time t for different values of N with $\rho = 1.0$ and $u = 0.05$.

is shown in Fig. 3 for the same values of the parameters that are used in Fig. 2. Therefore, a system without the ρ rescaling behaves as a usual one dimensional short-range interacting system and always remains paramagnetic.

We also see a dynamical slowing down with the range of the interactions when the system size is kept fixed, while the parameter ρ_0 is increased, maintaining scaling $\rho = \rho_0 N^2$. This is demonstrated using the evolution of cumulative magnetization and of kurtosis κ defined as

$$\kappa(t) = \frac{1}{3}\frac{\frac{1}{t}\int_0^t \langle p^4(t')\rangle dt'}{\frac{1}{t}\int_0^t \langle p^2(t')\rangle^2 dt'}, \tag{28}$$

where the average $\langle \ldots \rangle$ is over all the spins. For the BG equilibrium state $\kappa(t) \to 1$ as $t \to \infty$. The time series for $M(t)$ and kurtosis $\kappa(t)$ are shown in Figs. 4(a) and 4(b) respectively. As ρ_0 increases, both M and κ take a longer time to relax to their respective equilibrium values, indicating dynamical slowing down with increasing range of interaction.

In Fig. 5 we show that the system relaxes to the same final magnetization independent of the initial condition which is, again, a characteristic of the thermodynamic equilibrium.

Finally, in Fig. 6 we show the short time dynamics of relaxation of SCISM to the ferromagnetic state. Similar to the coarsening dynamics of systems with short-range interactions, the relaxation dynamics is algebraic, very different from the exponential relaxation to a ferromagnetic QSS observed in the HMF model [16]. This suggests that the ferromagnetic state to which the system evolves is a true equilibrium and not a ferromagnetic QSS.

B. Equilibrium properties

The mapping between the SCISM and the reduced model described in Sec. II shows that if SCISM relaxes to equilibrium, then the properties of the equilibrium state should be identical to those of the reduced model described by the effective Hamiltonian, Eq. (24). The difficulty is to establish if the stationary state to which the system relaxes is a true equilibrium state or a QSS. To explore this we again perform the numerical integration of the equations of motion Eqs. (6)–(9) as described in the previous section. We also numerically integrate the Hamilton's equations of motion for the reduced model, Eq. (24), to compare with the results obtained for the SCISM, Eq. (1).

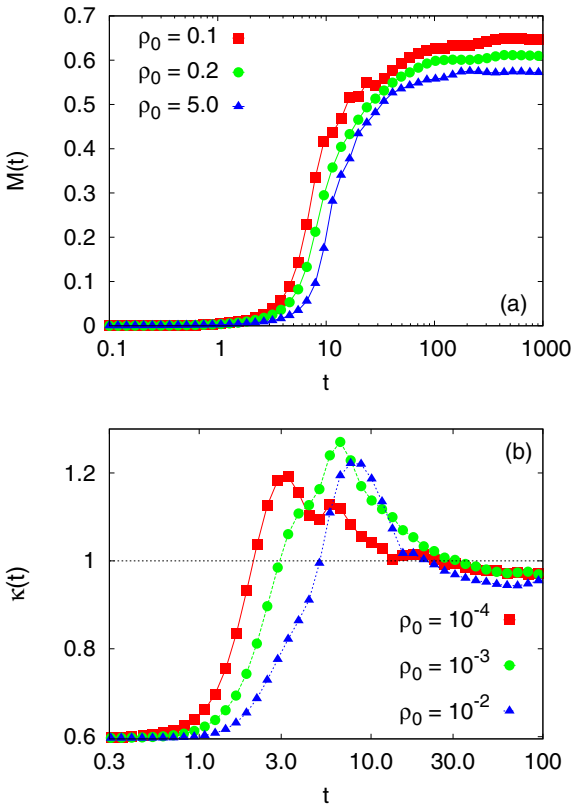

FIG. 4. (a) Evolution of the magnetization $M(t)$ with time t for different values of ρ_0 with $N = 100$ and $u = 0.02$. (b) Evolution of the kurtosis $\kappa(t)$ with time t for different values of ρ_0 with $N = 500$ and $u = 0.02$.

If the conjecture presented in the previous section is true, then SCISM, under suitable rescaling of the magnetic field coupling constant $\rho = \rho_0 N^2$, should exhibit a phase transition from a paramagnetic to ferromagnetic phase, similar to the equilibrium phase transition in the HMF model. To demonstrate the existence of the phase transition in our model, we numerically compute the average magnetization M as a function of the energy density for different sizes $N = 16, 32, 128$, with the rescaling $\rho = \rho_0 N^2$. We see in Fig. 7(a) that for small (large) u the magnetization M is large (small) and there is a

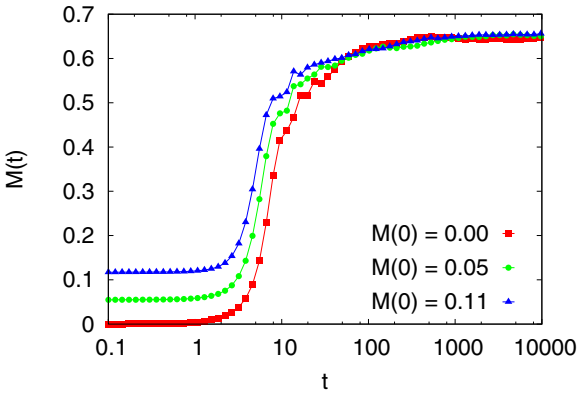

FIG. 5. Evolution of the magnetization with time t for three different initial conditions, all with the same energy $u = 0.02$, $\rho_0 = 0.1$, and $N = 100$.

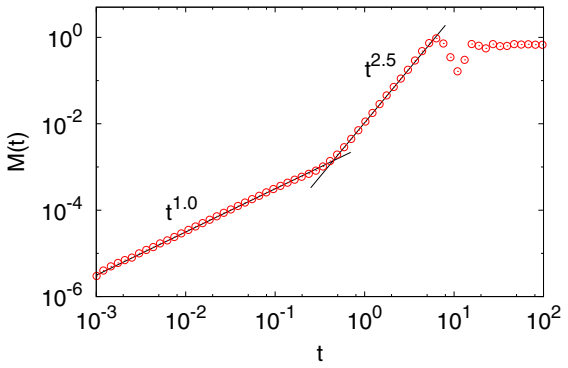

FIG. 6. Short time dynamics of $M(t)$ evolution to the magnetized state. Note that the algebraic behavior is very different from the exponential instability observed in the HMF model.

critical value of $u = u_c \approx 0.2$ which separates these two regions. As N increases the transition becomes more prominent, indicating that the phase transition persists as $N \to \infty$.

We also obtain the magnetization M vs u data by molecular dynamics using a symplectic Verlet velocity algorithm of the reduced Hamiltonian Eq. (24), and compare it with the same for the original model. For the reduced model the parameter α is obtained from the saturation value of the momentum $\langle p \rangle$ of the original model ($\alpha = -\langle p \rangle$) as has been argued in Sec. II and numerically shown in Fig. 1(a) for a few representative u values. We find that the two models show very good agreement over a wide range of u values, as can be seen in Fig. 7(b), indicating equilibrium phase transition, which is also consistent with the saturation of kurtosis at the value appropriate for the BG statistics show in Fig. 4(b).

We next compute the susceptibility χ defined as

$$\chi = N(\overline{m^2} - \overline{m}^2), \tag{29}$$

where the bar corresponds to the time average, for different system sizes N. The data for χ are shown in Fig. 8(a) as a function of the energy density u for $N = 32,64,128$. We see a susceptibility peak at energy close to $u = u_c$, with the peak height scaling as $N^{0.35}$, see inset of Fig. 8(a), indicating a thermodynamic second order phase transition. The susceptibility of the SCISM and of the reduced Hamiltonian once again show good agreement and both predict a phase transition at the same critical $u = u_c$; see Fig. 8(b).

Thus we have shown that the SCISM with the proper scaling $\rho = \rho_0 N^2$ shows dynamical and equilibrium properties similar to the globally coupled HMF model. A finite system relaxes to the thermodynamic equilibrium, as dictated by the BG statistics, but in the $N \to \infty$ limit the system will fail to equilibrate, and will remain trapped in a paramagnetic QSS, similar to what is observed for the HMF model. Finite N SCISM has a second order equilibrium phase transition from a paramagnetic to a ferromagnetic phase similar to what is seen in the HMF model, however, differently from the HMF which also has a first order nonequilibrium paramagnetic to

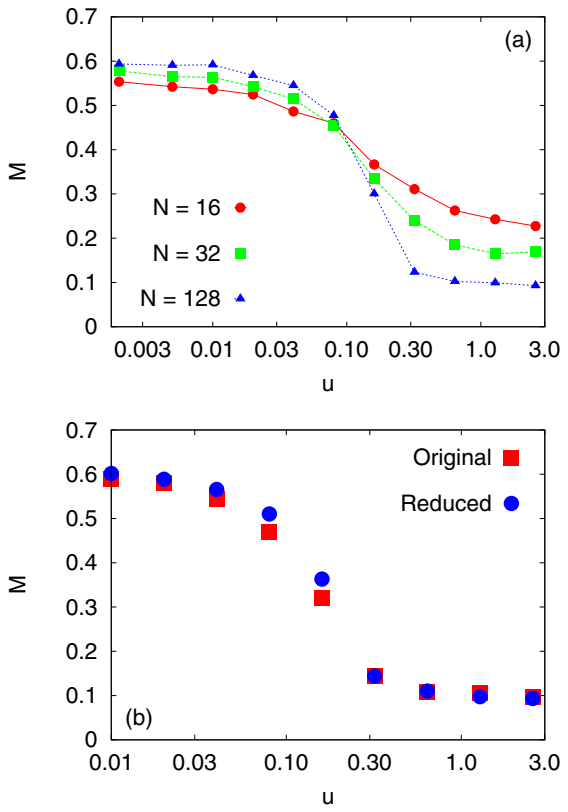

FIG. 7. (a) Variation of the cumulative magnetization M as a function of energy density u for different values of N. Here $\rho = \rho_0 N^2$ with $\rho_0 = 0.02$. (b) Comparison of the magnetization for the SCISM with the reduced model for $N = 100$.

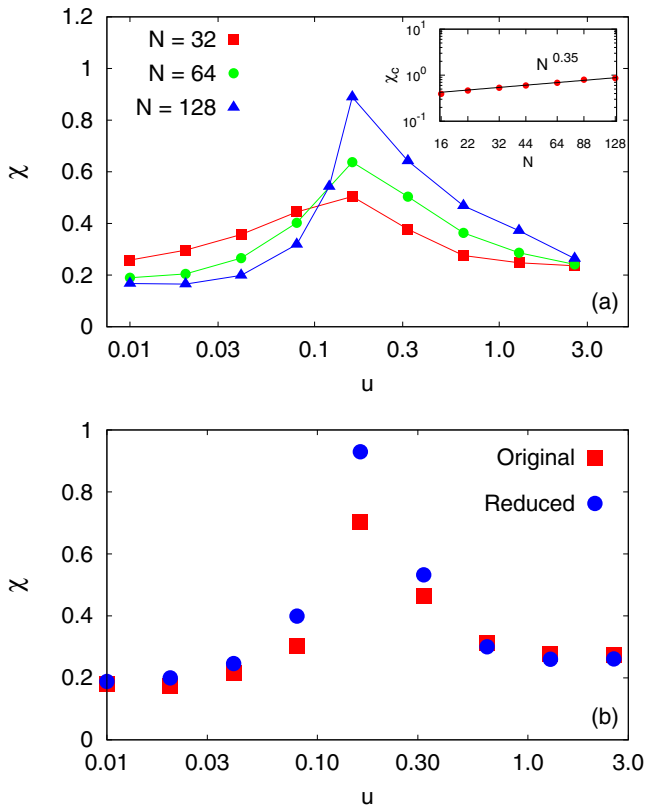

FIG. 8. (a) Variation of the susceptibility χ with the energy density u for different values of N. Here $\rho = \rho_0 N^2$ with $\rho_0 = 0.02$. Inset shows the scaling of the peak height with N. (b) Comparison of the susceptibility of the SCISM with the reduced model for $N = 100$.

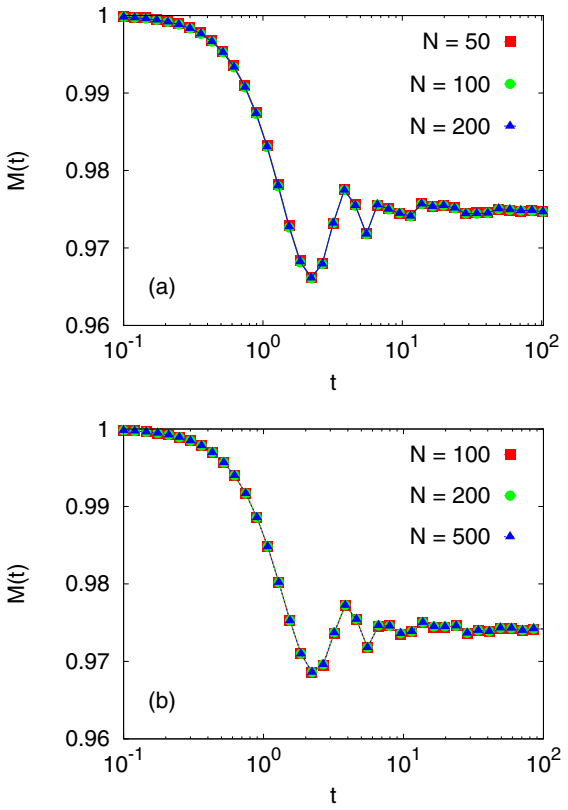

FIG. 9. Evolution of the magnetization $M(t)$ with time t for different values of N: (a) SCISM with $\rho_0 = 1$ and (b) the HMF model, both for $u = -0.45$. To compare the energy per particle of SCISM with HMF we have subtracted an additive constant $N/2$ conventionally introduced in the HMF Hamiltonian.

ferromagnetic phase transition [17], we do not observe any nonequilibrium magnetized QSSs in the SCISM. To see if the failure to find nonequilibrium magnetized QSSs is due to the initial condition, we now initialize our system with all the spins aligned, so that the initial magnetization is $m(t=0)=1$. The initial magnetic fields is $(h_x,h_y)=(1,0)$, while spin velocities are chosen from a uniform distribution as before. The magnetization time series for different system sizes are shown in Fig. 9(a). As can be seen, the magnetization appears to relax directly to its final equilibrium value at large times without becoming trapped in a QSS. We also verified that the final state corresponds to the thermodynamic equilibrium by computing the kurtosis κ, as described in Eq. (28). At late times the kurtosis relaxes to $\kappa \approx 1$, indicating that ferromagnetic state is, indeed, a true thermodynamic equilibrium. In Fig. 9(b) we show the same scenario for the HMF model under identical initial conditions—the magnetization time series appears to behave very similarly, qualitatively and even quantitatively. This leads us to speculate that failure to observe magnetized QSSs in the SCISM might be due to the smallness of the system sizes that we could study in our simulations.

IV. CONCLUSION

We have introduced a self-consistent interacting spin model in which spins interact through the magnetic field that they produce. The interaction through the field avoids a problem of instantaneous action at a distance. The dynamics of the magnetic field in the SCISM is identical to the one found in a FEL. Using analytical and numerical calculations we showed that by rescaling the magnetic field inhomogeneity coupling parameter, our locally interacting model behaves akin to the paradigmatic Hamiltonian mean-field model. Similar to the HMF model, we find an equilibrium paramagnetic to ferromagnetic phase transition. Furthermore, we observed that the lifetime of the paramagnetic state scales with $N^{1/3}$, so that in the thermodynamics limit the system initialized in a paramagnetic state will stay in this state forever, even for very low energies. Unfortunately, we were not able to see any ferromagnetic QSS states in the SCISM—all the ferromagnetic states that we have observed corresponded to a true thermodynamic equilibrium. We speculate that the reason for this failure is that the system sizes which we could explore with the computational resources available to us are too small to observe nonequilibrium QSSs.

ACKNOWLEDGMENTS

This work was partially supported by the CNPq, INCT-FCx, and by the US-AFOSR under Grant No. FA9550-16-1-0280.

[1] T. Padmanabhan, Phys. Rep. **188**, 285 (1990).
[2] R. H. French *et al.*, Rev. Mod. Phys. **82**, 1887 (2010).
[3] A. Campa, T. Dauxois, and S. Ruffo, Phys. Rep. **480**, 57 (2009).
[4] F. Bouchet, S. Gupta, and D. Mukamel, Physica A **389**, 4389 (2010).
[5] Y. Levin, R. Pakter, F. B. Rizzato, T. N. Teles, and F. P. C. Benetti, Phys. Rep. **535**, 1 (2014).
[6] S. Gupta and S. Ruffo, Int. J. Mod. Phys. A **32**, 1741018 (2017).
[7] M. Antoni and S. Ruffo, Phys. Rev. E **52**, 2361 (1995).
[8] A. Pluchino, V. Latora, and A. Rapisarda, Phys. Rev. E **69**, 056113 (2004).
[9] W. B. Colson, Phys. Lett. A **59**, 187 (1976).
[10] R. Bonifacio, C. Pellegrini, and L. M. Narducci, Opt. Commun. **50**, 373 (1984).
[11] J. Barré, T. Dauxois, G. De Ninno, D. Fanelli, and S. Ruffo, Phys. Rev. E **69**, 045501(R) (2004).
[12] A. Antoniazzi, D. Fanelli, S. Ruffo, and Y. Y. Yamaguchi, Phys. Rev. Lett. **99**, 040601 (2007).
[13] A. Antoniazzi, D. Fanelli, J. Barré, P. H. Chavanis, T. Dauxois, and S. Ruffo, Phys. Rev. E **75**, 011112 (2007).
[14] W. H. Press, B. P. Flannery, S. A. Teukolsky, and W. T. Vetterling, *Numerical Recipes in C: The Art of Scientific Computing* (Cambridge University Press, Cambridge, England, 1988).
[15] T. M. Rocha Filho, M. A. Amato, A. E. Santana, A. Figueiredo, and J. R. Steiner, Phys. Rev. E **89**, 032116 (2014).
[16] T. N. Teles, F. P. da C. Benetti, R. Pakter, and Y. Levin, Phys. Rev. Lett. **109**, 230601 (2012).
[17] R. Pakter and Y. Levin, Phys. Rev. Lett. **106**, 200603 (2011).